Morphology and Evolution in Galaxy Clusters I: Simulated Clusters in the Adiabatic limit and with Radiative Cooling

Nurur Rahman[1], Sergei F. Shandarin[1], Patrick M. Motl[2], and Adrian L. Melott[1]

[1] *Department of Physics and Astronomy, University of Kansas, Lawrence, KS 66045, USA;*
[2] *Center for Astrophysics and Space Astronomy, University of Colorado, Boulder, CO 80309, USA;*
nurur@kusmos.phsx.ukans.edu, sergei@ku.edu, motl@casa.colorado.edu, melott@kusmos.phsx.ukans.edu

arXiv:astro-ph/0405097v1 5 May 2004

ABSTRACT
We have studied morphological evolution in clusters simulated in the adiabatic limit and with radiative cooling. Cluster morphology in the redshift range, $0 < z < 0.5$, is quantified by multiplicity and ellipticity. In terms of ellipticity, our result indicates slow evolution in cluster shapes compared to those observed in the X-ray and optical wavelengths. The result is consistent with Floor, Melott & Motl (2003). In terms of multiplicity, however, the result indicate relatively stronger evolution (compared to ellipticity but still weaker than observation) in the structure of simulated clusters suggesting that for comparative studies of simulation and observation, sub-structure measures are more sensitive than the shape measures. We highlight a few possibilities responsible for the discrepancy in the shape evolution of simulated and real clusters.

Key words: clusters: morphology - clusters: structure - clusters: evolution - clusters: statistics

1 INTRODUCTION

The hierarchical clustering is the most popular model for the Large Scale Structure (LSS) formation. The model relys on the assumption that the larger clumps of matter distributions result due to the merging of smaller sub-clumps in cosmological time. Structural evolution in cosmological systems such as galaxies and clusters of galaxies is therefore the underlying principle in this scenario.

Melott, Chambers & Miller (2001; hereafter MCM) has reported evolution in the gross morphology of galaxy-clusters (quantified by ellipticity) for a variety of optical and X-ray samples over the redshift, $z < 0.1$. They infer that the evidence is consistent with low matter density universe. Using ellipticity as well as intracluster medium temperature and X-ray luminosity, Plionis (2002) has presented evidence for the recent evolution in optical and X-ray cluster of galaxies for redshift, $z \leq 0.18$. In both studies evolution is quantified by the change of cluster ellipticity with redshift. In a recent study, Jeltema et al. (2003) have reported structural evolution of clusters with redshift where cluster morphology is quantified by power ratio method (Buote & Tsai 1995). The authors used a sample of 40 X-ray clusters over the redshift range $0.1 - 0.8$ obtained from Chandra Observatory. The results of these previous studies, although each one employed different techniques in their analyses, indicate evolution in the morphology of the largest gravitationally bound systems over a wide range of look-back time.

The observational evidences prompted concerns on the formation and evolution of structures in numerical simulations. If the results of simulations give us faithful representations of the evolutionary history of cosmological objects than one would expect a similar trend in the structure of simulated objects. So far almost all studies of simulated clusters are focused on understanding the nature of the background cosmology within which the present universe is evolving (Jing et al. 1995; Crone, Evrard & Richstone 1996; Buote & Xu 1997; Valdarnini, Ghizzardi & Bonometto 1999). Until recently a comparative study of morphological evolution in the simulated and real clusters was absent. Floor et al. (2003) and Floor, Melott & Motl (2003; hereafter FMM) have investigated evolution in clusters morphology simulated with different initial conditions, background cosmology, and different physics (e. g., simulation with and without radiative cooling). They have used eccentricity as a probe to quantify evolution. Their studies, emphasizing on measuring shapes in the outer regions of clusters, suggest slow evolution in simulated cluster shapes compared to the observed clusters.

In this paper we study evolution in simulated clusters in flat cold dark matter universe (ΛCDM; $\Omega_m = 0.3$, $\Omega_\lambda = 0.7$) by using high resolution simulations (Motl et al. 2003). We use two data sets: the first set have clusters simulated in the adiabatic limit and the other set contains clusters simulated with radiative cooling. Each sample contain X-ray and dark matter distributions and has been analyzed at four different redshifts, $z = 0.0, 0.10, 0.25$, and 0.50.

This is the first in a series of papers aimed to study the

morphology and evolution of clusters of galaxies. The papers will use shape measure such as ellipticity derived from the Minkowski functionals (Minkowski 1903; hereafter MFs). The MFs provide a non-parametric description of the images implying that no prior assumptions are made on the shapes of the images. The measurements based on the MFs appear to be robust and numerically efficient when applied to various cosmological studies, e. g., galaxies, galaxy-clusters, CMB maps etc. (Mecke, Buchert & Wagner 1994; Schmalzing et al. 1999; Beisbart 2000; Beisbart, Buchert & Wagner 2001; Beisbart, Valdarnini & Buchert 2001; Kerscher et al. 2001a, 2001b; Sheth et al. 2003; Shandarin, Sheth & Sahni 2003). Various measures, derived from the two-dimensional scalar, vector and several tensor MFs to quantify shapes of galaxy images, had been described and tested in Rahman & Shandarin (2003a, 2003b; hereafter RS1 and RS2). The multiplicity, however, is not constructed from the MFs (see section §3 for details of parameter construction).

In this paper we use the extended version of the numerical code used in RS1 and RS2. In the following paper in this series we will analyze simulated clusters with cooling and heating mechanism such as star formation and star formation with supernovae feedback. We will also make a comparative study of observed and simulated clusters with up to date samples of optical and X-ray clusters.

The organization of the paper is as follows: simulation technique is described in §2, a brief discussion of shape measures is given in §3. The results are presented in §4 and the conclusions are summarized in §5.

2   NUMERICAL SIMULATIONS

We have analyzed projected clusters (in all three axes) simulated in the standard, flat cold dark matter universe (ΛCDM) with the following parameters: $\Omega_b = 0.026$, $\Omega_m = 0.3$, $\Omega_\lambda = 0.7$, $h = 0.7$, and $\sigma_8 = 0.928$ (Motl et al. 2003). We have used two samples of clusters derived from the same initial conditions and background cosmology. The major difference between the samples is in energy lose mechanism experience by the baryonic fluids. In one sample, the fluid is allowed to lose energy via radiation and subsequently cool; in the other sample no energy lose is allowed.

The simulations use a coupled N-body Eulerian hydrodynamics code (Norman & Bryan 1999; Bryan, Abel & Norman 2000) where the dark matter particles are evolved by the adaptive particle-mesh, N-body code. The PPM scheme (Colella & Woodward 1984) is used to treat the fluid component on a comoving grid. An adaptive mesh refinement (AMR) is employed to concentrate the numerical resolution on the collapsed structures that form naturally in cosmological simulations. The dark matter particles exist on the coarsest three grids; each sub-grid having twice the spatial resolution in each dimension and eight times the mass resolution relative to its parent grid. At the finest level, each particle has a mass of 9×10^9 h^{-1} M$_\odot$. A second order accurate TSC interpolation is used for the adaptive particle mesh algorithm. Up to seven levels of refinement are utilized for the fluid component, yielding a peak resolution of 15.6 h^{-1} kpc within the simulation box with sides of length 256 h^{-1} Mpc at the present epoch.

Since fluid is allowed to radiatively cool, a tabulated cooling curve (Westbury & Henriksen 1992) for a plasma of fixed, 0.3 solar abundance has been used to determine the energy loss to radiation. The cooling curve falls rapidly for temperatures below 10^5 K and is truncated at a minimum temperature of 10^4 K. Heat transport by conduction is neglected in the present simulation since it has been shown that even a weak, ordered magnetic field can reduce conduction by two to three orders of magnitude from the Spitzer value (Chandran & Cowley 1998). However, Narayan & Medvedev (2001) has shown that if the chaotic magnetic field fluctuations extends over a sufficiently large length scales within the intra-cluster medium (ICM), then thermal conductivity becomes significant to the global energy balance of the ICM. Energy input into the fluid from supernovae feedback or discrete sources such as AGN are also neglected in the current simulations. For a complete description of simulation in the adiabatic limit and with radiative cooling see Motl et al. (2003).

The adiabatic and radiative cooling samples, respectively, have 43 and 41 clusters in three dimension. Therefore we have a total of 129 (N_{ad}) and 123 (N_{rc}) projected clusters in the respective samples. Each projected cluster image is within a 8 h^{-1} Mpc (comoving) frame containing 360 × 360 pixels.

3   MORPHOLOGICAL PARAMETERS

We use multiplicity (M) and ellipticity (ϵ) as quantitative measures to study evolution in simulated clusters. Ellipticity is derived from the area tensor, a member of the MFs. The details on the MFs can be found in Schmalzing (1999), Beisbart (2000), and RS1. Here we discuss briefly the construction of the measures.

• Multiplicity (M): This parameter is defined as,

$$M = \frac{1}{A_{max}} \sum_{i=1}^{N} A_i, \tag{1}$$

where A_i is area of the individual components at a given level and A_{max} is the area of the largest component at that level, and N is the total number of components. It is a measure with fractional value and gives the number of components measured at any brightness level: $M = 1$ for a single iso-intensity contour (i. e. component) and $M > 1$ for multi-contours. Multiplicity is different than the Euler Characteristic (χ), a member of the scalar MFs (see RS1 for more). The EC is an integer number that gives the total number of components present at any given level but does not provide any information regardless of their sizes. Multiplicity, on the other hand, is able to extract this information.

It may be mentioned here that Thomas et al. (1998) have also used multiplicity as a parameter for sub-structure measure in N-body simulations. They define it as a ratio of mass of sub-clumps to cluster mass. In this study it is a ratio of the areas as defined in equation 1.

We use two variants of M to present our results: one is the average of multiplicity over all density/brightness levels, $\bar{M}_{eff}$, and the other is the maximum of the multiplicity found at one of the levels, M_{max}.

• Ellipticity (ϵ): We adopt the definition of ellipticity,

$$\epsilon = 1 - b/a, \tag{2}$$

where a and b are the semi-axes of an ellipse. For our purpose the semi-axes correspond to the "auxiliary ellipse" constructed from the eigenvalues of the area tensor (see RS1 for detail). We have used two variations of ϵ: one is sensitive to the shape of the individual cluster components present at a given level while the other is sensitive to the collective shape formed by all the components present at that level. We label these two variants of ϵ, respectively, as the effective (ϵ_{eff}) and the aggregate (ϵ_{agg}) ellipticity. Morphological properties of clusters such as shape and the nature or the degree of irregularity existing in these systems can be probed effectively with these two parameters.

At any given density/brightness level, we construct ϵ_{eff} as,

$$\epsilon_{eff} = \frac{1}{M \cdot A_{max}} \sum_{i=1}^{N} \epsilon_i \; A_i, \qquad (3)$$

where ϵ_i are ellipticities of the individual iso-intensity contours measured as stated earlier and M is the multiplicity at that level. The symbols A_i and A_{max} have similar meanings as before.

To construct ϵ_{agg}, we take the union of all components present at a given level and form a collective region. The integrated region can be expressed as

$$R = R_1 \cup R_2 \cup \cdots \cup R_N, \qquad (4)$$

where R_i is the region enclosed by each component. Subsequently we find the components of the area tensor and the "auxiliary ellipse" for the region R.

It is worth mentioning that the behavior of ϵ_{agg} is similar to conventional ellipticity measure based on inertia tensor (Carter & Metcalf 1980). But the construction procedure of these two measures are different. The conventional method finds the eigenvalue of the inertia tensor for an annular region enclosing mass density or surface brightness, on the other hand, the method based on MFs finds the eigenvalues of regions enclosed by the contour(s) is assumed to be homogeneous.

We have expressed ellipticities after averaging the estimates at all density/brightness levels. Our final result is, therefore, expressed by $\bar{\epsilon}_{eff}$ and $\bar{\epsilon}_{agg}$ rather than ϵ_{eff} and ϵ_{agg}.

3.1 Toy Models

To get a better feeling of the parameters mentioned above we provide an illustrative example with toy models. One can think of these toy models as snap shots of different X-ray clusters in projection taken at one particular time. We include clusters with different types of internal structures in Fig. 1: unimodal elliptic structure (panel 1), asymmetric and symmetric bimodal clusters (panels 2 and 3, respectively), cluster with filamentary structure (panel 4) etc. The multimodal clusters have clumps with different peak brightness. We show contour plots of toy models at different brightness levels where the choice of levels is arbitrary. For all clusters the outer line represents the percolation level at which substructures merge with one another forming a single, large system.

Multiplicity as a function of area (in grid unit) is shown in Fig. 2. As mentioned earlier M is sensitive to the sizes of the substructures. The simplest case to check this is to take a bimodal cluster. For a bimodal structure with unequal sized sub-clumps (panel 2), the fractional value of multiplicity ($1 < M < 2$) tells us that the components of the system have different sizes. The isolated components eventually percolate giving $M = 1$ at low brightness level, i. e, at larger area. On the other hand, for a cluster with equal components $M = 2$ until percolation occurs (panel 3). For clusters with three components (panels 4 and 5), we see that for a short range of brightness levels the components are well separated where two of these are bigger then the third one ($2 < M < 3$). Afterwards two of the three clumps merge giving $1 < M < 2$. These two remaining components eventually percolate to become a single system. The clumps in panel 6 are distributed around the center. For this cluster, we see two unequal size but well separated clumps ($1 < M < 2$) with same peak brightness. The behavior of clusters in panels 7 and 8 is similar except that they have different number of substructures. The cluster in panel 9 has the largest number of components (a total of 7). Two of its clumps are so large compared to the other ones that they dominant mostly. The multiplicity is always in the range $1 < M < 3$ reflecting the merging of clumps at different levels.

Ellipticity as a function of area is shown in Fig. 3. In this figure the solid and dotted line represent, respectively, ϵ_{agg} and ϵ_{eff}. For the unimodal cluster in panel 1, $\epsilon_{eff} = \epsilon_{agg}$. For the bimodal cluster in panel 2, the estimate of ϵ_{eff} gives an ellipticity weighted more by the larger component. In this case it is zero. However, for a bimodal system with equal sized sub-clumps but different elongation, ϵ_{eff} will give an average elongation of the two. The estimate of ϵ_{agg}, on the other hand, tells us about the overall shape of that system irrespective of the sizes and elongations of its sub-clumps. Due to the presence of two isolated components, the system itself appears more elongated than the shape of its sub-clumps.

The important point to note that the estimate provided by ϵ_{agg} depends not only on the relative sizes of the components but also on their relative separation. This is reflected in all panels containing multi-clump clusters. With the decrease of brightness, as the clumps get bigger and appear close to one another, ϵ_{agg} gets smaller.

For a multi-component system with filamentary structure, $\epsilon_{eff} < \epsilon_{agg}$ (panel 4). If components are distributed around the cluster center, $\epsilon_{eff} > \epsilon_{agg}$ (panel 6). The cluster in panel 5 has the unique property that is shown separately by clusters in panel 4 and 6. In transition from peak brightness to lower level, the cluster changes its filamentary shape to the one where the components are distributed over a region around the center. The ϵ_{agg} profile in panel 8 shows that in the range, $2.2 < \log_{10} A_S < 2.8$, the cluster develops two, almost equal size clumps that are very close to each other. Cluster in panel 7 follows the behavior of a bimodal cluster except that there is jump in between $2.6 < \log_{10} A_S < 2.8$ where the cluster changes its structure having two unequal size clumps to two equal size clumps. The shape of the cluster in panel 9 changes consistently following the merging of its clumps at different brightness.

3.2   Example of Simulated Clusters

We demonstrate the behaviors of M and the variants of ϵ as a function of area for several simulated clusters (Figs. 4 and 5). For each sample we choose two clusters at each redshift for illustration purpose. We use dark and gray lines to represent matter and X-ray clusters, respectively. Fig. 4 shows that both matter and X-ray clusters with cooling have higher number of sub-clumps than those without cooling. Fig. 5 shows that in most cases the central part of clusters consists of single peak ($\epsilon_{eff} = \epsilon_{agg}$). The central region of these clusters do not appear spherical. Rather the region appears to have some degree of flattening. We see that multi-peak systems, mostly bimodal clusters with un-equal size sub-clumps ($\epsilon_{eff} < \epsilon_{agg}$), are not uncommon for these clusters. In low brightness levels, i. e., in the outer regions of cluster, the sub-clumps appear to be homogeneously distributed ($\epsilon_{eff} > \epsilon_{agg}$).

4   RESULTS

The objective of this paper is to study morphological evolution in simulated cluster using M and ϵ as quantitative measures. The parameters represent the shape characteristics of a set of iso-intensity contours corresponding to a set of density/brightness levels. The levels represent equal interval in area (i.e. size) in log space. We select the range of area in between $30 \sim 35000$ (in grid unit) with 100 intervals. The lower limit is to avoid the discreteness of the grid whereas the upper limit covers the significant part of the entire image of each cluster analyzed. In fact with this range we can analyze clusters from ~ 80 h^{-1} kpc up to a distance ~ 2 h^{-1} Mpc. We do not smooth either the cluster image or its iso-intensity contours.

4.1   Comparison between Cluster Samples

The probability and cumulative distribution functions of these parameters determined from the cluster samples are shown in Figs. 6 to 9. In each of these figures the probability function (i. e., frequency normalized by the number of elements within the sample) are shown at the top two panels at 4 different redshifts. The cumulative functions are shown at the bottom two panels where dotted, dashed, long dashed, and solid lines are used for the cumulative functions derived at $z = 0.0, 0.10, 0.25$, and 0.50, respectively. In these figures dark and gray lines represent, respectively, $\bar{M}_{eff}$ and M_{max}; similarly dark and gray lines represent, respectively, $\bar{\epsilon}_{eff}$ and $\bar{\epsilon}_{agg}$. As mentioned earlier these parameters provide estimate averaged over 100 brightness levels.

From a visual examination of the distribution functions in Figs. 6 to 9 one can notice an evolutionary trend in cluster morphology since the gross properties of clusters indeed change with redshifts. Our goal is to determine the statistical significance of this trend and than compare it with the observation. We should mention that multiplicity as defined here had not been used before. It is, therefore, not possible to make a direct comparison with other studies or observations. As a result we will use only ellipticity for comparison with observations. We will explore the robustness and sensi-

tivity of M in our future work on Sloan Digital Sky Survey (SDSS) clusters.

To check whether or not the trend is significant, we have performed K-S test between cumulative functions at two different z for each parameter. The test is repeated for all combinations of redshifts and the results are presented in the tables 1 to 4 where d and p represent the K-S statistic and significance level probability. The tables show test results only for those redshift combinations that may indicate a significant evolution, i. e., only those results for which p < 0.1. Recall that a small value of p corresponds to a significant difference between two distribution functions.

In terms of M, the test results give a strong indication of evolution when cumulative functions at different z are compared (Figs. 6 and 7; tables 1 and 2). The distribution functions of ϵ, on the other hand, show slow or very weak evolution. (Figs. 8 and 9; tables 3 and 4). This is a general outcome for both samples of clusters.

Figs. 6 and 7 show that clusters in the cooling sample have a higher value of multiplicity at all redshifts compared to those in the adiabatic sample. The low abundance of single component systems with radiative cooling indicates that the dense, cool core substructures are long lived features (Motl et al. 2003).

Table 1 shows the K-S tests of the distributions of M and M_{max} for adiabatic clusters. From the table we find that these clusters, in general, show marked decline in sub-clumps from $z = 0.50, 0.25$ to $z = 0.0$ (p $\simeq 10^{-4}$). In between $z = 0.10$ and $z = 0.0$, the evolution is less significant (p $\simeq 10^{-2}$).

Table 2 shows that the evolution of dark matter clusters in the cooling sample is stronger compared to the X-rays. The low significance is a reflection of less efficient merging in the X-ray gas. In fact in terms of M_{max}, the X-ray clusters do not show any significant change in the distribution functions over redshift. For dark matter, the distribution functions of this parameter do evolve from $z = 0.50, 0.25$ to $z = 0.0$.

The distribution functions of ellipticities for both samples are shown in Figs. 8 and 9. We see that the X-ray clusters, in general, are more regular than those of dark matter. The X-ray gas evolves in the dark matter potential and due to the radiation pressure it is distributed homogeneously in the background. As a result the morphological characteristics of systems containing baryonic fluids will be more regular. For these clusters the irregular components are distributed over a region instead of concentrating along one direction making them appear regular. A comparison of $\bar{\epsilon}_{eff}$ with $\bar{\epsilon}_{agg}$ for dark matter clusters shows that the sub-clumps are not distributed homogeneously around the central region. Rather these clumps are spread out mostly in one direction forming filamentary structure, as indicated by the larger value of $\bar{\epsilon}_{agg}$.

No significant evolution is signaled by $\bar{\epsilon}_{eff}$ either for matter or for X-ray clusters in the adiabatic sample (table 3). It indicates that the shape of individual components of a cluster at one redshift may appear similar at other redshifts. Since $\bar{\epsilon}_{eff}$ puts emphasize on individual components, therefore, it is not unusual to see no evolution quantified by this parameter. In terms of $\bar{\epsilon}_{agg}$, we see that the overall shapes of X-ray clusters do evolve from $z = 0.50, 0.25$ towards $z = 0.0$ (p $\simeq 10^{-5}$). The matter clusters, however,

show less significant evolution ($p \simeq 10^{-2}$) from $z = 0.50$ to $z = 0.0$.

Once again no evolution is signaled by $\bar{\epsilon}_{eff}$ for clusters with radiative cooling (table 4). We see a moderate evolutionary trend is given by $\bar{\epsilon}_{agg}$ from $z = 0.50$ to $z = 0.10$ and 0.0 with $p \simeq 10^{-3}$.

As a final check with the distribution functions, we take projection along each axis at a time and repeat the K-S tests. Recall that in this case sub-samples (along each axis) have 41 clusters in the adiabatic limit and 43 clusters with radiative cooling. The results of these sub-samples show insignificant variation from the bigger primary sample. Therefore, it is less likely that the overall result is affected by projection effect.

We present redshift evolution of the measures for adiabatic and cooling sample in Figs. 10 and 11, respectively. At each redshift we show the median and the mean with 1σ error bar derived from the distribution functions. We quantify the rate of evolution by the slope of the line obtained from the best least-squares fit to the M vs. z and ϵ vs. z relationship shown in these figures where rate means either dM/dz or $d\epsilon/dz$. The solid and dashed lines represent the best fit to the data given, respectively, by the median and the mean. We summarize our measurements in tables 5 and 6.

Several conclusions can be drawn from these tables. First, the dark matter shows very similar evolution in both samples of clusters. Second, the X-ray clusters in adiabatic simulation evolve faster than those with radiative cooling. Third, the rate of ellipticity evolution is higher for X-ray clusters irrespective of cooling history. Fourth, as far as the strength of evolution is concerned, multiplicity, especially M_{max}, appears to be more sensitive indicator than ellipticity.

We note that the measured quantities for the dark matter in the adiabatic and cooling cluster samples are very similar. This is a check on the consistency of the simulations and analysis. The result is expected as the N-body segment of the simulations are identical in the two cluster samples with the exception of the gas that has relatively minor contribution to the total gravitational potential. The LSS of adiabatic and cooling clusters are generally similar but their small scale structures are dictated by the overall cluster properties rather than perturbative interactions (Motl et al. 2003). In adiabatic clusters infalling sub-clumps mix into the main cluster medium in a faster manner relative to the radiative cooling where sub-clusters can be long lived. This is the reason behind fast evolution of adiabatic X-ray clusters. The relaxation times scale for collisionless particles is much longer than that of the collisional gas particles (Frenk et al. 1999; Valdarnini, Ghizzardi & Bomometto 1999). Therefore matter clusters will appear not only more elongated than the X-ray gas distribution but the redshift evolution of their shapes will also be slow. More spherical configuration for X-ray clusters is also expected from the point of view that intracluster gas is in hydrostatic equilibrium whereas the dark matter is distributed like galaxies (Kolokotronis et al. 2001).

FMM have analyzed the same sets of simulated clusters in the redshift range $0.0 - 0.25$ using eccentricity (e) as the quantitative measure. The eccentricity is defined as, $e = \sqrt{1 - \lambda_2/\lambda_1}$ where λ_1 and λ_2 are eigenvalues of the inertia tensor ($\lambda_1 > \lambda_2$). Note that the eigenvalues are proportional to the square of the semi-axes of an ellipse. FMM used moment of inertia technique for an annular region to calculate e. The size of the annulus is fixed either by r_{outer} or r_{200} where r_{outer} is the 1.5 h^{-1} Mpc aperture and the r_{200} is the radius from cluster center up to a distance where the density is ~ 200 times the background.

To make a comparison with FMM, we measure eccentricity for our data sets. Using both effective ($\bar{e}_{eff}$) and aggregate ($\bar{e}_{agg}$) eccentricities, we find that 1) the results agree, at least, qualitatively in the slow evolution of simulated clusters and 2) both studies show that clusters without cooling evolve faster compared to those having radiative cooling in a Λ dominated universe.

However, we note two systematic differences between the results. First, our results show that matter distributions generally are more elongated than the X-ray gas whereas in FMM both of these systems have comparable eccentricities. As mentioned earlier the collisionless dark matter distribution relaxed in longer time than the hot gas, it seems unlikely that both systems will have comparable flattening within the same cosmological time slot (i. e., $0 < z < 0.5$). Second, at each redshift our estimates are higher compared to those of FMM. FMM focuses mainly to determine the shape in the outer region of galaxy-clusters. Our method, on the other hand, measures shapes from the central regions towards the edge of clusters (up to ~ 2 h^{-1} Mpc). In cluster morphology it is important to know which part of a cluster needs to be analyzed that will give a realistic estimate of its shape. For example, to study clusters with cool core one should include the central region in the analysis to see to what extent it influences the overall shape since cooling is is a small scale phenomenon that occurs within 100 to 200 h^{-1} kpc of cluster center. Emphasizing only on the outer part for cool core clusters, therefore, may not reflect the estimate of actual shape. Clusters with or without cooling appear to be more elongated around the central region (see Fig. 5; note that a similar trend in simulated cluster without cooling has also been reported by Jing & Suto 2002). Since we estimate an average eccentricity, our result is weighted more by the large flattening around the central part. The difference in results is, therefore, a reflection of different methodology.

4.2 Comparison with Observed Clusters

The optical sample of MCM has 138 ACO clusters with $z < 0.1$. It has been compiled from West & Bothun (1990); Rhee, van Haarlem & Katgert (1991) and Kolokotronis et al. (2001). We do not see any evolution for this sample ($d\epsilon/dz \sim 0.03$). Plionis (2002) has the largest sample of optical clusters with measured ellipticity. It has 407 APM clusters with $z < 0.18$. For our purpose this sample is slightly better than the MCM since it has clusters with higher redshift. Besides, ~ 30 clusters of this sample are also present in the MCM. The rate of evolution for this sample is $d\epsilon/dz \sim 0.7$. However, if both are combined, replacing the common ones by the APM clusters, the rate increases. The combined sample of ~ 500 optical clusters with $z < 0.18$ shows $d\epsilon/dz \sim 1.06$.

It is rare to find a large sample of X-ray clusters with up-to-date ellipticity measure. We use the sample of MCM that is compiled from Mcmillan, Kowalski & Ulmer (1989)

and Kolokotronis et al. (2001). It only has 48 clusters with $z < 0.1$ which is three times smaller than the MCM optical sample and an order of magnitude smaller than the APM. It also has low redshift limit than the APM. The rate of evolution for this sample is $d\epsilon/dz \sim 1.7$. The result suggests faster evolution for X-ray clusters than the opticals. Although the result is in accordance with our expectation, we should not make any definite conclusion because of the size of the sample. A large sample of X-ray clusters with better selection criteria and extended over wide redshift is needed to be conclusive.

We reanalyze the APM clusters and the combined sample imposing redshift cutoff $z < 0.1$ in order to have redshift range consistent with the MCM X-ray sample. These samples show, respectively, $d\epsilon/dz \sim 1.02$ and ~ 1.0. Even though evolution of optical clusters gets faster in this redshift range, it is still slower than that of the X-rays.

When we compare the rate of evolution between simulated and observed cluster ellipticity, we find slower evolution in simulations. In spite of this, it is interesting that the simulation is able to capture the essence of reality: faster evolution of gas than the dark matter distribution.

5 CONCLUSIONS

Numerical simulations provide an unique opportunity to understand the underlying physics of structure formation. In order to be representative of the real world, the results from simulations should agree with observations. Observations provide evidence of morphological evolution in galaxy-clusters (Melott, Chambers & Miller 2001; Plionis 2002; Jeltema et al. 2003), simulations should show similar evolution. With this in mind, we have studied redshift evolution of cluster morphology simulated, respectively, in the adiabatic limit and with radiative cooling.

Since observed clusters are projected along the line of sight and lack of full 3 dimensional information we, therefore, use projected simulated clusters. Each cluster image is within a 8 h^{-1} Mpc frame containing 360×360 pixels. The clusters are analyzed at 100 different density/brightness levels using multiplicity and ellipticity as two different probes to quantify morphological evolution.

Our results show that if cluster shapes are quantified by ellipticity, than simulations do not model the observed local universe well enough. The results indicate that the simulated clusters do evolve with redshift but the evolution is slower than the observed one. The outcome of our analyses, however, should be taken with a caution since the measurements from different samples do not agree to be conclusive on the slower evolution. Take, for example, the optical clusters for $z < 0.1$: the APM sample shows $d\epsilon/dz \sim 1.02$, whereas the MCM sample shows $d\epsilon/dz \sim 0.03$. A recent study by Flin, Krywult & Biernacka (2004; hereafter FKB) reports very weak evolution for a sample of 246 ACO clusters for redshift range $0 < z < 0.3$. They analyze clusters at five different annular radii and the mean of these estimates shows $d\epsilon/dz \sim 0.013$. For $z < 0.1$, their result also indicates weak evolution (Flin, 2004). In terms of ellipticity, therefore, we can see clearly from table 5 and 6 that the evolution is slower for both sets of simulations with respect to the APM sample but it is stronger compared to both MCM and FKB.

A preliminary analysis of a sample of 800 clusters constructed from the SDSS shows that ellipticity evolution of optical clusters within $z < 0.1$ is weaker than that of the APM clusters. The result also shows that clusters with different mass limits evolves differently. Large, massive clusters ($M \sim 10^{15} M_\odot$) have stronger evolution compared to the less massive clusters ($M \sim 10^{13} - 10^{14} M_\odot$) (Miller 2004). The sample is uniform with a well documented selection function and high degree of completeness. If this is the case then we can infer that the cluster samples mentioned above have less uniformity in mass range: the APM catalogue is biased towards the massive cluster and both MCM and FKB samples contain less massive clusters. Note that we have checked the evolution in simulated clusters with the mass limits as mentioned above but have not found any difference.
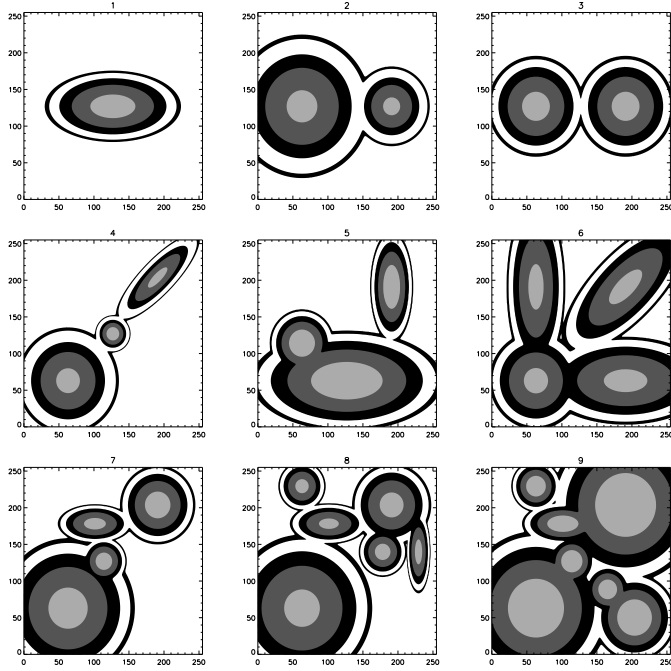
The discrepancy in the optical samples is an indication of different selection criteria used to construct the catalogues. Larger and more complete catalogues obtained from Sloan Digital Sky Survey and XMM-Newton survey may be able to shed more light into this issue. It is also likely that numerical simulations may lack crucial physics that needs to be included (see FMM for discussion). In the forthcoming paper in this series we will analyze cluster samples simulated with various gas physics, for example, star formation and feedback from supernovae explosion. The result of that study may give some clue to gain better insight of the discrepancy.

Finally, our result indicates that multiplicity (M_{max}) indicates relatively stronger evolution in cluster morphology compared to ellipticity This particular result suggests that it is a more sensitive parameter than ellipticity (see also Thomas et al. 1998; Suwa et al. 2003). We will further explore the sensitivity of this measure in our future work on simulation and observed clusters.
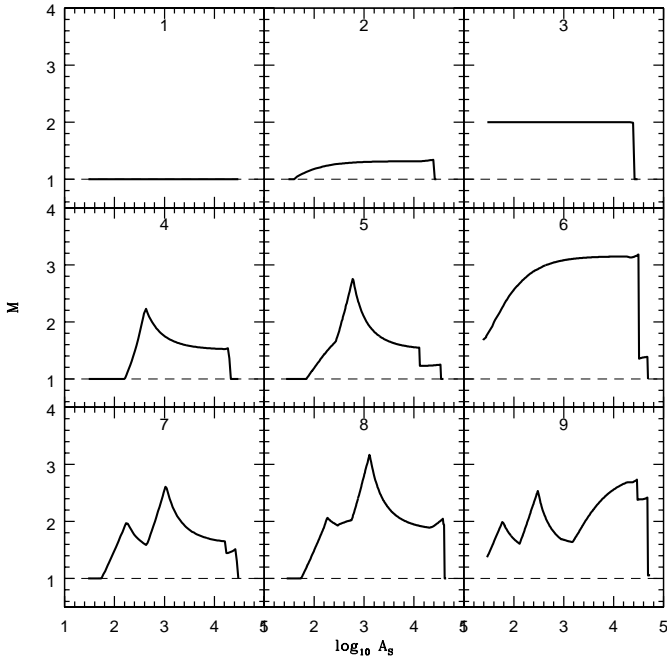
REFERENCES
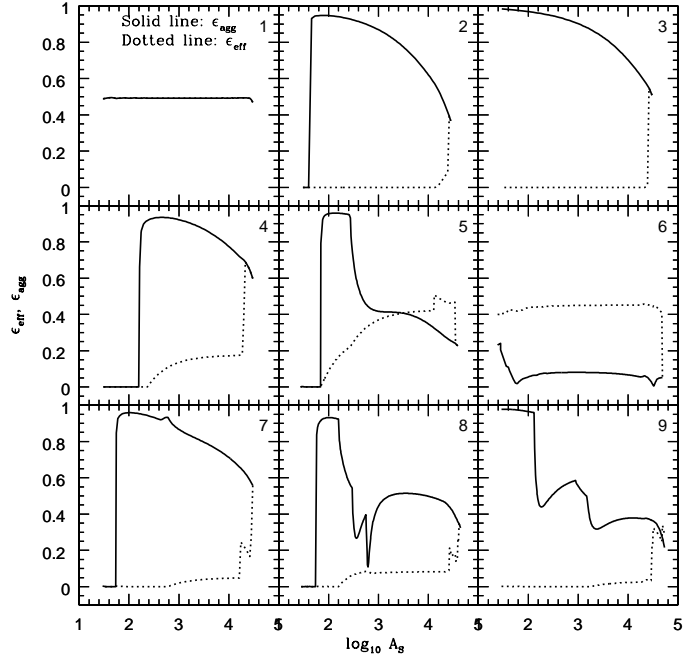
Beisbart C., 2000, Ph.D. Thesis, Ludwig-Maximilians-Universität, München, Germany
Beisbart C., Buchert T., Wagner H., 2001, Physica A, 293, 592B
Beisbart C., Valdarnini R., Buchert T., 2001, A&A, 379, 412
Bryan G. L., Abel T., Noramn M. L., 2001, Proceedings of Supercomputing, http://www.sc2001.org/
Buote D. A., Tsai J. C., 1995, ApJ, 452, 522
Carter D., Metcalfe N., 1980, MNRAS, 191, 325
Chandran B. D. G., Cowley S. C., 1998, Phys. Rev. Lett. 80, 3077
Colella P., Woodward P. R., 1984, J. Comput. Phys., 54, 174
Flin P., Krywult J., Biernacka M., 2004, astro-ph/0404182 (FKB)
Flin P., 2004, private communication
Floor S. N., Melott A. L., Miller C. J., Bryan G. L., 2003, ApJ, 591, 741
Floor S. N., Melott A. L., Motl P. M., 2003, astro-ph/0307539, in press ApJ (FMM)
Frenk C. S. et al., 1999, ApJ, 525, 554

Figure 1. Contour plots of toy clusters at different brightness levels. The choice of levels is arbitrary. The multi-modal clusters have clumps with different peak brightness. For all clusters the outer line represents the percolation level at which substructures merge and form a single, large system.

Figure 3. Ellipticity as a function of area for toy models. The number at each panel corresponds to the cluster number shown in Fig. 1. The solid and dotted line represent, respectively, ϵ_{agg} and ϵ_{eff}. For details see text.
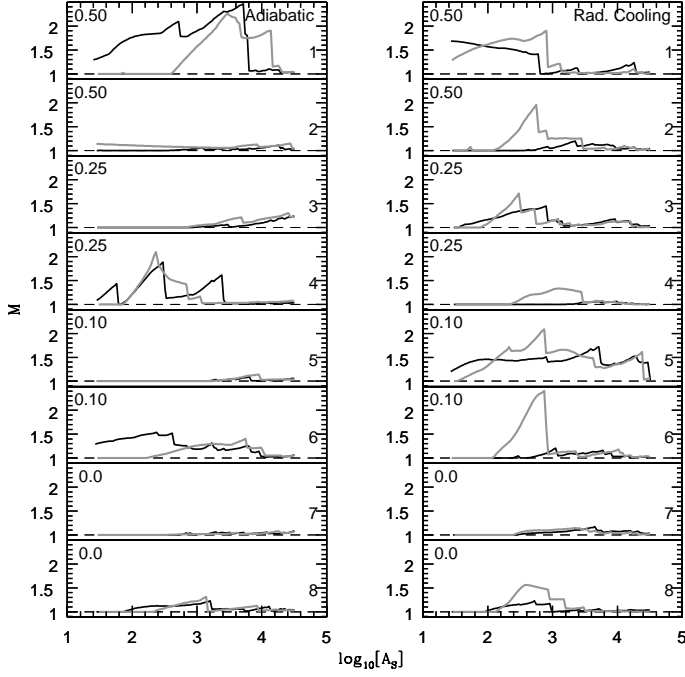

Figure 2. Multiplicity as a function of area for toy models. The number at each panel corresponds to the cluster number shown in Fig. 1. For details see text.

Hobson M. P., Jones A. W., Lasenby A. N., 1999, MNRAS, 309, 125

Jeltema T. E., Canizares C. R., Bautz M. W., Buote D. A., 2003, astro-ph/0310124

Jing Y. P., Mo H. J., Börner G., Fang L. Z., 1995, MNRAS, 276, 417

Jing Y. P., Suto Y, 2002, ApJ, 574, 538

Kerscher M., Mecke K., Schmalzing J., Beisbart C., Buchert T., Wagner H., 2001a, A&A, 373, 1

Kerscher M. et al., 2001b, A&A, 377, 1

Kolokotronis V., Basilakos S., Plionis M., Georgantopoulos I., 2001, MNRAS, 320, 49

Mecke K. R., Buchert T., Wagner H., 1994, A&A, 288, 697

Miller C. J., 2004, private communication

Minkowski H., 1903, Math. Ann., 57, 447

Motl P. M., Burns J. O., Loken C., Norman M. L., Bryan G., 2003, astro-ph/0302427

Narayan R., Medvedev M. V., 2001, ApJ, 562, L129

Norman M. L., Bryan G. L., 1999, ASSL Vol. 240: Numerical Astrophysics, eds. Miyama S. M., Tomosaka K., Hanawa T., (Boston, Kluwer), 19

Rhee G. F. R. N., van Haarlem M., Katgert P., 1991, A&AS, 91, 513

Rahman N., Shandarin S. F., 2003a, MNRAS, 343, 933 (RS1)

Rahman N., Shandarin S. F., 2003b, astro-ph/0310242 (RS2)

Schmalzing J., 1999, Ph.D. Thesis, Ludwig-Maximilians-Universität, Münichen, Germany

Schmalzing J., Buchert T., Melott A. L., Sahni V., Sathyaprakash B. S., Shandarin S. F., ApJ, 526, 568

Sheth J. V., Sahni V., Shandarin S. F., Sathyaprakash B. S., 2003, MNRAS, 343, 22S

Shandarin S. F., Sheth J. V., Sahni V., 2003, astro-ph/0310112

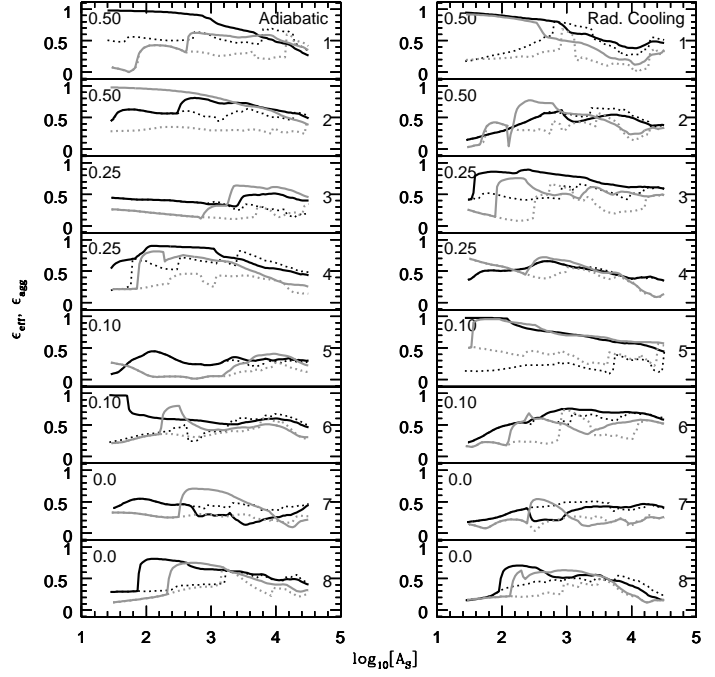Suwa T., Habe A., Yoshikawa K., Okamoto T., 2003, ApJ, 588, 17

Figure 4. The multiplicity (M) as a function of area (A_S) for a selection of clusters at $z = 0.50, 0.25, 0.10$, and 0.0. Two clusters from each redshift are shown. The dark and gray solid lines represent the matter and X-ray clusters, respectively. For a uni-modal cluster, $M = 1$, on the other hand for a multi-modal cluster, $M > 1$. Figure shows that multiplicity is, in general, greater than 1 in the entire redshift range for clusters simulated with radiative cooling (right panels) indicating a slower evolution than in the adiabatic sample (left panels).

Thomas P. A. et al., 1998, MNRAS, 296, 1061

Valdarnini R., Ghizzardi S., Bomometto S., 1999, New Astronomy, 4, 71

West M. J., Bothun G. D., 1990, ApJ, 350, 36

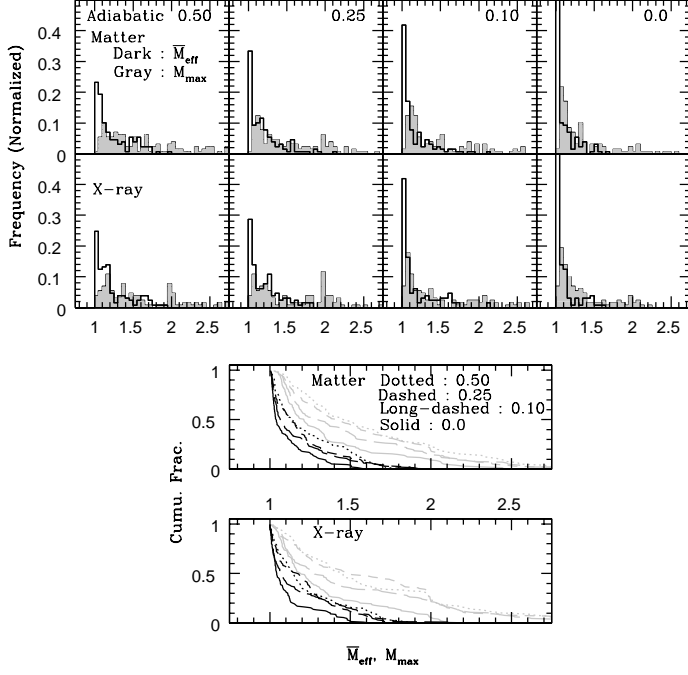Westbury C. F., Henriksen R. N., 1992, ApJ, 338, 64

Figure 5. The effective (ϵ_{eff}) and aggregate (ϵ_{agg}) ellipticity as a function of area (A_S) for the same clusters as in Fig. 4. Dotted and solid lines are used for ϵ_{eff} and ϵ_{agg}, respectively. The matter and X-ray clusters are shown, respectively, by the dark and gray lines. In most cases the central part of clusters consists of single peak (i. e., $\epsilon_{eff} = \epsilon_{agg}$). The central region of these clusters do not appear spherical. Rather the region appears to have some degree of flattening. Multi-peak systems, mostly bimodal clusters with un-equal size sub-clumps ($\epsilon_{eff} < \epsilon_{agg}$), however, are not uncommon. At low brightness levels, i. e., in the outer regions of cluster, the sub-clumps appear to be homogeneously distributed ($\epsilon_{eff} > \epsilon_{agg}$).

Table 1. Multiplicity in the adiabatic sample. The K-S test result between cumulative distribution functions at different redshifts for $\bar{M}_{eff}$ (top) and M_{max} (bottom). In the tables z, d, and p stand for redshift, K-S statistics, and the significance level probability, respectively. In K-S test, a small value of the probability suggests that two distributions are different from each other.

z	Matter		X-ray	
	d	p	d	p
0.00 - 0.10	0.17	4.1×10^{-2}	0.18	2.9×10^{-2}
0.00 - 0.25	0.26	3.3×10^{-4}	0.33	7.3×10^{-7}
0.00 - 0.50	0.33	1.5×10^{-6}	0.34	3.7×10^{-7}
0.10 - 0.25	0.18	2.9×10^{-2}	0.18	2.9×10^{-2}
0.10 - 0.50	0.22	3.7×10^{-3}	0.22	3.7×10^{-3}
0.25 - 0.50	-	-	-	-

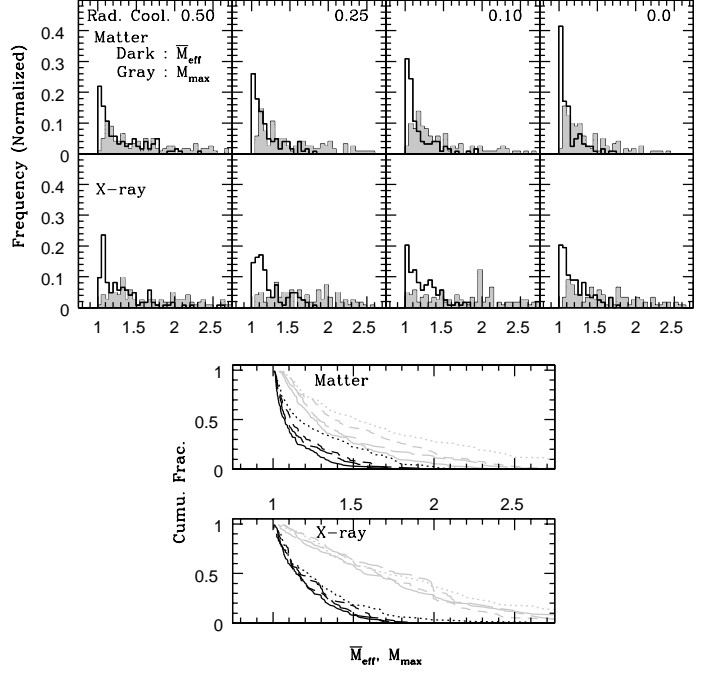| z	Matter		X-ray	
	d	p	d	p
0.00 - 0.10	0.17	4.1×10^{-2}	0.17	4.1×10^{-2}
0.00 - 0.25	0.26	3.3×10^{-4}	0.30	1.9×10^{-5}
0.00 - 0.50	0.30	1.0×10^{-5}	0.30	1.0×10^{-5}
0.10 - 0.25	-	-	0.19	2.0×10^{-2}
0.10 - 0.50	0.22	2.4×10^{-3}	0.20	8.9×10^{-3}
0.25 - 0.50	-	-	-	-

Figure 6. Multiplicity in adiabatic sample. The figure shows the normalized frequency (probability distribution function; top two panels) and the cumulative fraction (cumulative distribution function; bottom two panels) of $\bar{M}_{eff}$ and M_{max} at different redshifts for matter and X-ray clusters. The total number of cluster in this sample is, $N_{ad} = 129$. The numbers at the top-right in the uppermost panels show the redshifts.

Figure 7. Multiplicity in radiative cooling sample. The normalized frequency (top two panels) and the cumulative fraction (bottom two panels) of $\bar{M}_{eff}$ and M_{max} at different redshifts for matter and X-ray clusters. The total number of cluster in this sample is, $N_{rc} = 123$.

Table 2. Multiplicity in the radiative cooling sample. The K-S test result between cumulative distribution functions at different redshifts for $\bar{M}_{eff}$ (top) and M_{max} (bottom).
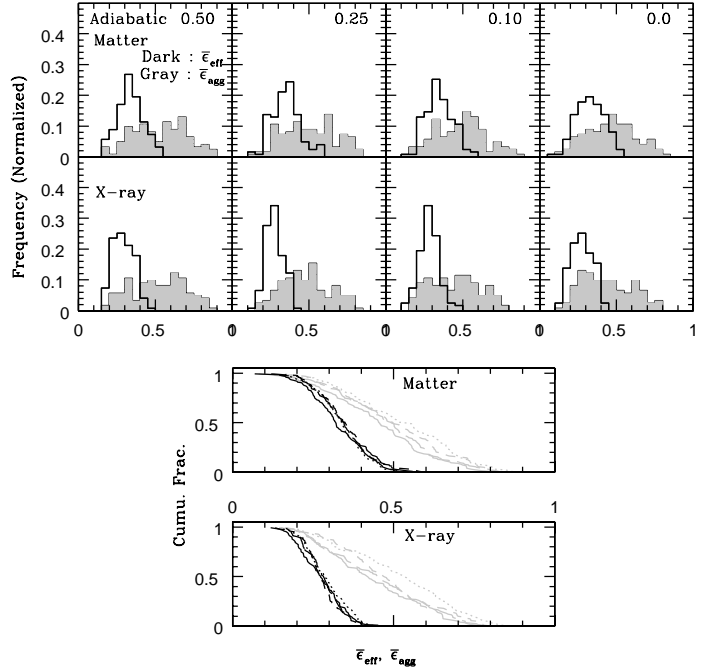
z	Matter		X-ray	
	d	p	d	p
0.00 - 0.10	-	-	-	-
0.00 - 0.25	0.17	4.9×10^{-2}	0.15	9.6×10^{-2}
0.00 - 0.50	0.26	3.6×10^{-4}	0.16	6.9×10^{-2}
0.10 - 0.25	-	-	-	-
0.10 - 0.50	0.20	1.0×10^{-2}	-	-
0.25 - 0.50	-	-	-	-

z	Matter		X-ray	
	d	p	d	p
0.00 - 0.10	-	-	-	-
0.00 - 0.25	0.20	1.0×10^{-2}	-	-
0.00 - 0.50	0.27	2.1×10^{-4}	-	-
0.10 - 0.25	-	-	-	-
0.10 - 0.50	0.22	4.4×10^{-3}	-	-
0.25 - 0.50	-	-	-	-

Figure 8. Ellipticity in adiabatic sample. The normalized frequency (top two panels) and the cumulative fraction (bottom two panels) of $\bar{\epsilon}_{eff}$ and $\bar{\epsilon}_{agg}$ at different redshifts for matter and X-ray clusters.
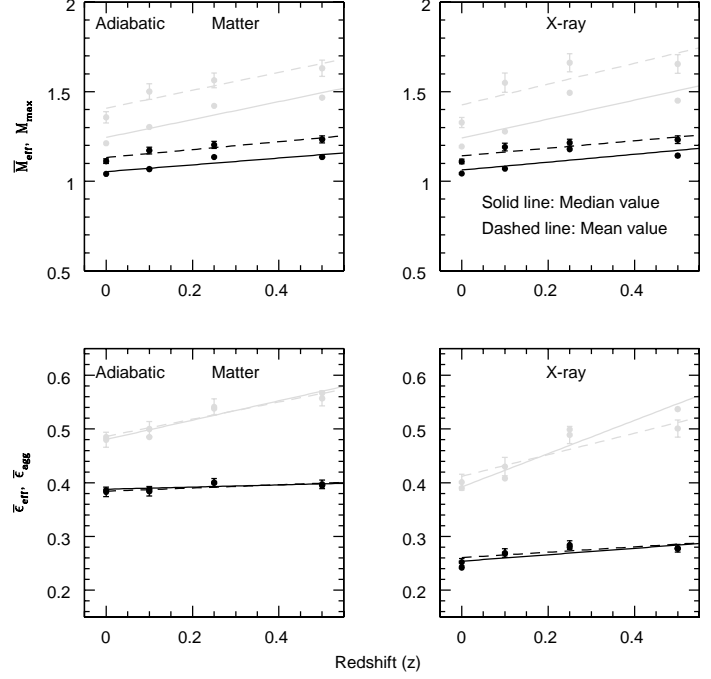
Figure 9. Ellipticity in radiative cooling sample. The normalized frequency (top two panels) and the cumulative fraction (bottom two panels) of $\bar{\epsilon}_{eff}$ and $\bar{\epsilon}_{agg}$ at different redshifts for matter and X-ray clusters.

Table 3. Ellipticity in the adiabatic sample. The K-S test result between cumulative distribution functions at different redshifts for ϵ_{eff} (top) and ϵ_{agg} (bottom).

z	Matter		X-ray	
	d	p	d	p
0.00 - 0.10	-	-	-	-
0.00 - 0.25	0.16	5.8×10^{-2}	0.18	2.9×10^{-2}
0.00 - 0.50	0.16	8.1×10^{-2}	-	-
0.10 - 0.25	-	-	-	-
0.10 - 0.50	-	-	-	-
0.25 - 0.50	-	-	-	-

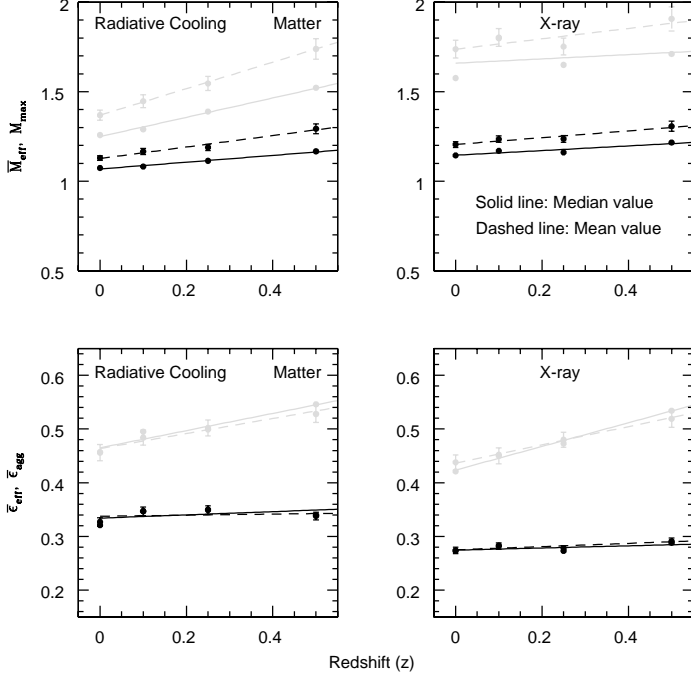| z	Matter		X-ray	
	d	p	d	p
0.00 - 0.10	-	-	0.18	2.9×10^{-2}
0.00 - 0.25	0.16	5.8×10^{-2}	0.29	3.5×10^{-5}
0.00 - 0.50	0.22	2.4×10^{-3}	0.29	1.9×10^{-5}
0.10 - 0.25	-	-	0.19	2.0×10^{-2}
0.10 - 0.50	0.16	5.8×10^{-2}	0.18	2.9×10^{-2}
0.25 - 0.50	-	-	-	-

Figure 10. Adiabatic sample: Redshift (z) evolution of M and ϵ for matter and X-ray clusters. At each redshift, the figure shows median, and mean with 1σ error bar derived from the probability distribution functions. The solid and dashed lines are the best fit lines, respectively, for median and mean (see table 5). The top panels show multiplicity where dark and gray lines are used for $\bar{M}_{eff}$ and M_{max}, respectively. The bottom panels show ellipticity where dark and gray lines are used for ϵ_{eff} and ϵ_{agg}, respectively.

Table 4. Ellipticity in the radiative cooling sample. The K-S test result between cumulative distribution functions at different redshifts for ϵ_{eff} (top) and ϵ_{agg} (bottom).

z	Matter		X-ray	
	d	p	d	p
0.00 - 0.10	-	-	-	-
0.00 - 0.25	-	-	0.16	6.9×10^{-2}
0.00 - 0.50	-	-	0.15	9.6×10^{-2}
0.10 - 0.25	-	-	-	-
0.10 - 0.50	-	-	-	-
0.25 - 0.50	-	-	-	-

z	Matter		X-ray	
	d	p	d	p
0.00 - 0.10	-	-	-	-
0.00 - 0.25	-	-	-	-
0.00 - 0.50	0.24	1.7×10^{-3}	0.25	6.2×10^{-4}
0.10 - 0.25	-	-	-	-
0.10 - 0.50	0.22	4.4×10^{-3}	0.20	1.0×10^{-2}
0.25 - 0.50	-	-	-	-

Figure 11. Radiative cooling sample: Redshift (z) evolution of M and ϵ for matter and X-ray clusters. Presentation style is similar to Fig. 10 except that this time table 6 is used to draw the best fit lines.

Table 6. The rate of evolution and the error in its measurement for clusters in the radiative cooling sample. The rate is obtained from M vs. z and ϵ vs. z relationship (Fig. 11) The presentation style is similar to table 5.

Parameter	Matter		X-ray	
	slope	error	slope	error
$\bar{M}_{eff}$	0.19	0.02	0.13	0.04
	0.32	0.04	0.19	0.04
M_{max}	0.54	0.03	0.12	0.30
	0.74	0.02	0.29	0.14
$\bar{\epsilon}_{eff}$	0.03	0.04	0.02	0.02
	0.01	0.03	0.03	0.01
$\bar{\epsilon}_{agg}$	0.16	0.03	0.22	0.02
	0.14	0.02	0.17	0.01

Table 5. The rate of evolution and the error in its measurement for clusters in the adiabatic sample. The rate is given by the slope of the line obtained from the least-square fit to M vs. z and ϵ vs. z relationship (Fig. 10). For each measure the 1st and 2nd row show the results obtained, respectively, from the median and the mean. The second column for each type of clusters shows the error estimated for the slope.

Parameter	Matter		X-ray	
	slope	error	slope	error
$\bar{M}_{eff}$	0.19	0.07	0.22	0.14
	0.22	0.06	0.21	0.09
M_{max}	0.50	0.13	0.53	0.27
	0.50	0.15	0.58	0.30
$\bar{\epsilon}_{eff}$	0.02	0.02	0.06	0.04
	0.03	0.02	0.05	0.03
$\bar{\epsilon}_{agg}$	0.18	0.04	0.31	0.07
	0.16	0.03	0.20	0.06